HHS Public Access

Author manuscript

Science. Author manuscript; available in PMC 2020 June 30.

Published in final edited form as:

Science. 2020 March 27; 367(6485): 1473–1476. doi:10.1126/science.aaz0251.

Ultrahigh-Field ^{67}Zn NMR reveals short-range disorder in zeolitic imidazolate framework glasses

Rasmus S.K. Madsen[1,†], **Ang Qiao**[1,†], **Jishnu Sen**[2], **Ivan Hung**[3], **Kuizhi Chen**[3], **Zhehong Gan**[3], **Sabysachi Sen**[2,*], **Yuanzheng Yue**[1,4,5,*]

[1]Department of Chemistry and Bioscience, Aalborg University, 9220 Aalborg, Denmark

[2]Division of Materials Science and Engineering, University of California at Davis, Davis, CA 95616, USA

[3]National High Magnetic Field Laboratory. 1800 E. Paul Dirac Drive Tallahassee, FL 32310

[4]State Key Laboratory of Silicate Materials for Architectures, Wuhan University of Technology, Wuhan 430070, China

[5]School of Materials Science and Engineering, Qilu University of Technology, Jinan 250353, China

Abstract

The structure of zeolitic imidazole framework (ZIF) melt-quenched glasses can provide insights into their glass formation mechanism. We directly detected short-range disorder in ZIF glasses using ultrahigh field zinc-67 solid-state nuclear magnetic resonance (NMR) spectroscopy. Two distinct Zn sites characteristic of the parent crystals transformed upon melting into a single tetrahedral site with a broad distribution of structural parameters. Moreover, the ligand chemistry in ZIFs appeared to have no controlling effect on the short-range disorder, although the former affected their phase transition behavior. These findings reveal structure-property relations and could help design metal-organic framework glasses.

One sentence summary:

Short-range structural disorder in ZIF glasses is detected, and ZIF melting relates to the loss of the symmetry of the tetrahedral Zn-ligand units.

*Corresponding Authors: yy@bio.aau.dk (Y.Z.Y.), sbsen@ucdavis.edu (S.S.).
†These authors equally contributed to this work.

Authors contributions: Y.Z.Y. and S.S. conceived the project; Y.Z.Y., S.S., R.S.M. and A.Q. made the outline of the project. I.H., K.C. and Z. G. performed NMR measurements at NHMFL. J.S. performed all NMR spectral data processing and simulation. A.Q., R.S.K.M and Y.Z.Y. synthesized the samples, and conducted DSC and XRD measurements. Y.Z.Y., S.S., R.S.M. and A.Q. wrote the manuscript with inputs from I.H., K.C., Z. G. and J.S..

Competing interests: The authors declare that they have no competing interests.

Data and materials availability: All data needed to evaluate the conclusions in the paper are present in the paper and/or the Supplementary Materials. Additional data related to this paper may be requested from the authors.

Supplementary Materials:
Materials and Methods
Figure S1–S5
Table S1–S3
SM refs (30-34)

Glasses can be obtained through a variety of synthesis and processing routes (1,2) but rapid cooling of the liquids remains the predominant approach. Melt-quenched (MQ) glasses can be broadly classified as inorganic, organic, and metallic and containing ionic-covalent, covalent and metallic bonds, respectively. Recently, a fourth family of MQ glasses based on metal-organic framework (MOF) have been reported that have coordinate bonds (3–7). The MQ-MOF glasses are primarily represented by the subset of MOFs called the zeolitic imidazolate frameworks (ZIFs). Their extended tetrahedral network is analogous to silica and zeolites (8): metal ion nodes (e.g., Zn^{2+}, Co^{2+}) substitute for silicon and imidazole (Im: $C_3N_2H_3$)-based ligands substitute for oxygen as the bridging unit. A number of ZIF glasses have porosity that has potential applications in gas capture and storage, and the ZIF-62 glass exhibits high transparency and broad mid-infrared luminescence that have potential photonic applications (7,9–13).

Recent studies have found ZIF-4 ($Zn[Im]_2$) and ZIF-62 ($Zn[Im_{2-x}bIm_x]$, where Im and bIm are imidazole and benzimidazole, respectively, to be rather stable against crystallization during heat-treatment, and that the parent liquids have a higher glass-forming ability compared to most of the network glass-forming liquids (14,15). The glass-forming ability of ZIF-62 is greater than that of ZIF-4, because its mixed linkers consisting of imidazole and benzimidazole in each tetrahedron create greater steric hindrance (14). Previous studies that explored the structural origin of this high glass-forming ability in both ZIF systems used systematic heat-treatments, differential scanning calorimetry (DSC), and x-ray pair distribution function (PDF) analyses (3,14,15). The PDF analyses provided no clear evidence of the appearance of any medium- or long-range order in these glasses after a calorimetric scan, despite the appearance of an exothermic peak immediately before melting (15). The enthalpy release was attributed to the densification of the structural network, but the nature and the length scale of the structural changes associated with the decrease of the potential energy remain unclear to date. In addition, although ZIF-4 is chemically simpler than ZIF-62, the former exhibits several features in its temperature-induced phase transitions, including the transition from low-density amorphous phase (LDA) to high-density amorphous phase (HDA), as well as the formation and melting of ZIF-zni (denser than ZIF-4).

The origin of these multiple transitions remains elusive given the limitations of the analytical techniques available for determining short- and intermediate-range structure in glasses. Raman spectroscopy, $^{13}C/^{1}H$ nuclear magnetic resonance (NMR) spectroscopy, along with x-ray PDFs, have been used in the past to study the short-range and medium-range structure of ZIF glasses. Although these studies provided some structural information, no substantial structural difference in the short-range order between the ZIF crystals and corresponding glasses could be identified (14). Previous studies showed that the organic ligands in ZIFs remained intact during melt-quenching, implying that the chemical integrity was retained after glass formation (3,5,14). Molecular dynamics simulations indicated that upon melting, the imidazolate linkers dissociate and reassociate with Zn atoms through the scission and renewal of Zn-N coordinate bonds (14,16). The $[ZnN_4]$ tetrahedral units remain intact in the ZIF glass state after the melt is quenched, and long-range structural disorder is believed to be primarily induced by the distortion of the ZnN_4 inter-tetrahedral connections (14,16).

In contrast, the short-range structural order at the scale of the Zn[ligand]$_4$ tetrahedra in MOF glasses remains unknown. Because ^{67}Zn is a quadrupolar nuclide, its NMR spectra can provide not only the information on the chemical shift that is characteristic of the tetrahedral environment of Zn in the ZIFs, but also on the electric-field gradient (EFG) at the site of this nuclide in the structure, as encoded in its quadrupolar coupling constant C_Q and asymmetry parameter η_Q. The EFG is a second-rank tensor quantity sensitive to the degree of positional and orientational order at length scales corresponding to the nearest and next-nearest neighbor distances, and possibly at further distances (17).

Only a few studies of ^{67}Zn NMR spectroscopy has been reported that analyzed crystalline structures in zinc-based compounds, including Zn-based crystalline MOFs (18–23), because the ^{67}Zn nuclide has a low gyromagnetic ratio, large quadrupole moment Q, as well as a low natural abundance (18). These issues, in combination with the low atomic density of MOFs, necessitated ^{67}Zn NMR spectral data collection at ultra-high magnetic fields that are ~20 T or higher. We report a comparative structural study of selected crystalline ZIFs and their glassy counterparts derived via melt-quenching, using ultra-high field ^{67}Zn magic-angle-spinning (MAS) NMR spectroscopy at 19.5 and 35.2 T at the National High Magnetic Field Laboratory.

The DSC traces of ZIF-4 and ZIF-62 samples (Fig. 1A) measured the temperature-driven enthalpic responses to the chemical reactions and phase transitions. During the first upscan (from 323 to 863 K), the as-synthesized ZIF-4 crystal underwent solvent release, amorphization, polymorphic transformation to ZIF-zni crystal, and finally melting. Subsequent quenching of the ZIF-zni melt resulted in the formation of a ZIF-4 glass with a T_g of 570 K during the second upscan. In contrast, during upscan 1, the as-synthesized standard ZIF-62 crystal displays the enthalpy responses corresponding only to the solvent release and the subsequent melting. After melt-quenching, the second upscan of ZIF-62 glass showed a glass transition with a T_g of 593 K.

To explore the effect of the linker chemistry (i.e., the Im/bIm ratio) on the short-range structure, we prepared a ZIF-62 crystal with a higher bIm content (denoted as ZIF-62b, see Table S1). Its XRD patterns confirmed that ZIF-62 and ZIF-62b had the same crystalline structure (Fig. S2). The final chemical compositions of ZIF-62 and ZIF-62b were $(Zn(Im)_{1.75}(bIm)_{0.25})$ and $Zn(Im)_{1.68}(bIm)_{0.32}$, as determined from ^{1}H liquid NMR measurements (Fig. S3). We also prepared a ZIF-62b glass sample by melt-quenching that was also subjected to two DSC scans. The increase of bIm in ZIF-62 framework led to an increase of both T_m and T_g (Fig. S4), consistent with a previous study (14). The XRD patterns of both crystal and glass samples for ZIF-4, -zni, and −62 (Fig. 1B) show the presence of long-range order in crystalline ZIFs and its absence in their glassy counterparts. The vitrification of these ZIF-crystals is schematically demonstrated in Fig. 1C.

The ^{67}Zn MAS NMR spectra of the three crystalline ZIFs (ZIF-4, ZIF-62, ZIF-zni) were obtained at two different magnetic fields, 19.5 and 35.2 T (Fig. 2). Each of these crystals contained two crystallographically distinct Zn sites at a 1:1 ratio, one of which is a more distorted ZnN_4 tetrahedron (18). The ^{67}Zn MAS NMR line shapes also necessitated simulation with at least two sites with subequal (within ±5%) relative fractions (Fig. 2); we

used the software Dmfit (24). For each composition, the spectra for each magnetic field were fitted simultaneously with the same set of NMR parameters: isotropic chemical shift δ_{iso}, the quadrupolar coupling constant C_Q and asymmetry parameter η_Q. These parameters are listed in Table 1 and the C_Q values for ZIF-4 are in good agreement with those reported in a recent study (18).

The data in Table 1 indicated that the δ_{iso} for all Zn sites in all materials varied over a rather narrow range from ~ 277 to 297 ppm. However, for each crystalline ZIF, the Zn sites (the less distorted Zn2) had a smaller C_Q of ~ 4.0 MHz and other (the more distorted tetrahedral Zn1) by a larger C_Q of ~ 5 to 6 MHz. These assignments followed the density functional theory-based calculations by Sutrisno et al. (18). Intriguingly, in spite of having the same composition, the ^{67}Zn C_Q values of the two Zn sites in ZIF-4 crystal are substantially different from those in ZIF-zni crystal. This result may be indicative of the corresponding difference in the topology between these two crystals; ZIF-4 has a *cag* topology and the ZIF-zni has a *zni* topology (5). The higher C_Q values of the Zn sites in the ZIF-zni crystal compared to those for the ZIF-4 crystal are also consistent with ZIF-zni possessing a greater variance in the bond angles and lengths for the Zn sites compared to ZIF-4 (Tables S2 and S3).

The ^{67}Zn MAS-NMR spectra of the ZIF-4 and ZIF-62 glasses obtained at 19.5 T and at 35.2 T (Figs. 3A–D). These spectra had asymmetric line shapes with low-frequency tails that we attributed to a continuous distribution of C_Q characteristic of structural disorder in the glassy state. These ^{67}Zn MAS NMR line shapes were well simulated with δ_{iso} (277 to 278 ppm) similar to that observed in corresponding crystals (288-297 ppm; see Table 1) and with a Czjzek distribution of the C_Q parameter (25), which yields a root-mean-square quadrupolar product $\sqrt{\langle C^2_{Q\eta} \rangle}$ of ~6.9 MHz for the ZIF-4 glass and ~6.5 to 6.8 MHz for the two ZIF-62 glasses. When taken together, the results in Table 1 indicate that as the ZIF crystals were melt-quenched into glass, the C_Q values increased and displayed a broader distribution, indicating that the structural disorder of the Zn[ligand]$_4$ tetrahedral environment in the glassy state was higher than that in the parent crystals. The ^{67}Zn NMR parameters for all three ZIF glasses were similar (Table 1), implying similar degree of short-range disorder, despite their differences in the Im/bIm ratio in the ligands.

The disappearance of the two distinct Zn sites characteristic of the ZIF crystals upon melting and vitrification indicates that the scission and renewal of the Zn-N bonds upon melting resulted in structural reconstruction (Fig. 1C, Fig. S1). With their three-dimensional network of corner-sharing [ZnN$_4$] tetrahedral units, ZIF glasses are structurally analogous to vitreous silica, but the coordinate bonding strength of ZIF glasses was weaker than covalent-ionic bonds found in silica (26, 27). The silica glass network would be more rigid than ZIF glasses, and the local structure of the former would be more ordered than that of ZIF-glasses. The bulky nature of the organic linkers in ZIF glasses could also cause steric hindrance, thus limiting the ability of the linker to return to its equilibrium position i.e., to the ordered structural state with lower potential energy, upon melt-quenching. The comparison in NMR spectra among ZIF-4 and -zni crystals and ZIF-4 glass (Fig. 3E), and between ZIF-62 crystal and glass (Fig. 3F) shows broadening of the glasses compared with

the crystals, and the resonance peaks moved to somewhat lower isotropic chemical shift from crystal to glass. While the increased broadening corresponds to a high degree of structural disorder in glasses at the short-range scale, the lowering of the isotropic chemical shift is suggestive of a change in the local coordination environment of Zn atoms upon vitrification. Previous Zn K-edge X-ray absorption fine structure and PDF measurements (5) indicated that Zn is in tetrahedral coordination with N in both glassy and crystalline ZIFs, and that the Zn-N distance did not change significantly upon vitrification. However, ^{67}Zn solid-state NMR results of Sutrisno et al. *(18)* showed that the ^{67}Zn NMR isotropic chemical shift of ZIF-14 (260 ppm) with longer Zn-N distances (2.00-2.02 Å) was significantly lower than that of ZIF-8 or ZIF-4 (300-315 ppm) characterized by shorter Zn-N distances (1.98-1.99 Å). Although further systematic studies are needed to establish this trend, the lower ^{67}Zn NMR isotropic chemical shift of ZIF glasses compared to their crystalline counterparts as observed in the present study could be an indication of an increase of the average Zn-N distance in the former, consistent with the corresponding increase in the molar volume upon vitrification.

Supplementary Material

Refer to Web version on PubMed Central for supplementary material.

Acknowledgments

Funding: The authors would like to thank the VILLUM FONDEN (No. 13253) and the NSFC (No. 51802263), China, for financial support. S.S. acknowledges support from the National Science Foundation grant NSF-DMR 1855176. The National High Magnetic Field Laboratory is supported by the National Science Foundation through NSF/DMR-1644779 and the State of Florida. Development of the 36 T SCH magnet and NMR instrumentation was supported by NSF (DMR-1039938 and DMR-0603042) and NIH (BTRR 1P41 GM122698).

References and Notes:

1. Angell CA, Formation of glasses from liquids and biopolymers. Science 267, 1924–1935 (1995). [PubMed: 17770101]
2. Greaves GN, Sen S, Inorganic glasses, glass-forming liquids and amorphizing solids. Adv. Phys. 56, 1–166 (2007).
3. Bennett TD, Tan J-C, Yue YZ, Baxter E, Ducati C, Terrill NJ, Yeung HH-M, Zhou Z, Chen W, Henke S, Hybrid glasses from strong and fragile metal-organic framework liquids. Nat. Commun. 6, 8079 (2015). [PubMed: 26314784]
4. Umeyama D, Funnell NP, Cliffe MJ, Hill JA, Goodwin AL, Hijikata Y, Itakura T, Okubo T, Horike S, Kitagawa S, Glass formation via structural fragmentation of a 2D coordination network. Chem. Commun. 51, 12728–12731 (2015).
5. Bennett TD, Yue YZ, Li P, Qiao A, Tao H, Greaves NG, Richards T, Lampronti GI, Redfern SAT, Blanc F, Farha OK, Hupp JT, Cheetham AK, Keen DA, Melt-quenched glasses of metal-organic frameworks. J. Am. Chem. Soc. 138, 3484–3492 (2016). [PubMed: 26885940]
6. Umeyama D, Horike S, Inukai M, Itakura T, Kitagawa S, Reversible solid-to-liquid phase transition of coordination polymer crystals. J. Am. Chem. Soc. 137, 864–870 (2015). [PubMed: 25530162]
7. Zhao YB, Lee SY, Becknell N, Yaghi OM, Angell CA, Nanoporous transparent MOF glasses with accessible internal surface. J. Am. Chem. Soc. 138, 10818–10821 (2016). [PubMed: 27539546]
8. Park KS, Ni Z, Côté AP, Choi JY, Huang R, Uribe-Romo FJ, Chae HK, O'Keeffe M, Yaghi OM, Exceptional chemical and thermal stability of zeolitic imidazolate frameworks. Proc. Natl. Acad. Sci. U. S. A. 103, 10186–10191 (2006). [PubMed: 16798880]

9. Zhou C, Longley L, Krajnc A, Smales GJ, Qiao A, Eruçar I, Doherty CM, Thornton AW, Hill AJ, Ashling CW, Qazvini OT, Lee SJ, Chater PA, Terrill NJ, Smith AJ, Yue YZ, Mali G, Keen DA, Telfer SG, Bennett TD, Metal-organic framework glasses with permanent accessible porosity. Nat. Commun. 9, 5042 (2018). [PubMed: 30487589]
10. Frentzel-Beyme L, Kloß M, Pallach R, Salamon S, Moldenhauer H, Landers J, Wende H, Debus J, Henke S, Porous purple glass – a cobalt imidazolate glass with accessible porosity from a meltable cobalt imidazolate framework. J. Mater. Chem. A 7, 985–990 (2019).
11. Frentzel-Beyme L, Kloss M, Kolodzeiski P, Pallach R, Henke S, Meltable mixed-linker zeolitic imidazolate frameworks and their microporous glasses - from melting point engineering to selective hydrocarbon sorption. J. Am. Chem. Soc. DOI: 10.1021/jacs.9b05558.
12. Ali MA, Ren JJ, Zhao TY. Liu XF, Hua YJ, Yue YZ, Qiu JR, Broad mid-infrared luminescence in a metal-organic framework glass. ACS Omega 4, 12081–12087 (2019). [PubMed: 31460321]
13. Qiao A, Tao HZ, Carson MP, Aldrich SW, Thirion LM, Bennett TD, Mauro JC, Yue YZ, Optical properties of a melt-quenched metal-organic framework glass. Opt. Lett. 44, 1623–1625 (2019). [PubMed: 30933106]
14. Qiao A, Bennett TD, Tao H, Krajnc A, Mali G, Doherty CM, Thornton AW, Mauro JC, Greaves GN, Yue YZ, A metal-organic framework with ultrahigh glass-forming ability. Sci. Adv. 4, eaao6827 (2018). [PubMed: 29536040]
15. Zhang JY, Longley L, Liu H, Ashling CW, Chater PA, Beyer KA, Chapman KW, Tao H, Keen DA, Bennett TD, Yue YZ, Structural evolution in a melt-quenched zeolitic imidazolate framework glass during heat-treatment. Chem. Commun. 55, 2521–2524 (2019).
16. Gaillac R, Pullumbi P, Beyer KA, Chapman KW, Keen DA, Bennett TD, Coudert F-X, Liquid metal–organic frameworks. Nat. Mater. 16, 1149 (2017). [PubMed: 29035353]
17. Kentgens APM, A practical guide to solid-state NMR of half-integer quadrupolar nuclei with some applications to disordered systems. Geoderma 80, 271 (1997).
18. Sutrisno A, Terskikh VV, Shi Q, Song Z, Dong J, Ding SY, Wang W, Provost BR, Daff TD, Woo TK, Huang Y, Characterization of Zn-containing metal–organic frameworks by solid-state ^{67}Zn NMR spectroscopy and computational modeling. Chem. - Eur. J 18, 12251–12259 (2012). [PubMed: 22945610]
19. Mroué KH, Power WP, High-field solid-state ^{67}Zn NMR spectroscopy of several zinc–amino acid complexes. J. Phys. Chem. A 114, 324–335 (2010). [PubMed: 19919076]
20. Bastow T, NMR in zinc metal. J. Phys.: Condens. Matter 8, 11309 (1996).
21. Wu G, Kroeker S, Wasylishen RE, Multinuclear NMR study of dipotassium tetracyanometalates of the group 12 metals in the solid state. Inorg. Chem. 34, 1595–1598 (1995).
22. Larsen FH, Lipton AS, Jakobsen HJ, Nielsen NC, Ellis PD, ^{67}Zn QCPMG solid-state NMR studies of zinc complexes as models for metalloproteins. J. Am. Chem. Soc. 121, 3783–3784 (1999).
23. Lipton AS, Heck RW, Ellis PD, Zinc solid-state NMR spectroscopy of human carbonic anhydrase: implications for the enzymatic mechanism. J. Am. Chem. Soc. 126, 4735–4739 (2004). [PubMed: 15070393]
24. Massiot D, Fayon F, Capron M, King I, Le Calvé S, Alonso B, Durand J-O, Bujoli B, Gan Z, Hoatson G, Modelling one- and two-dimensional solid-state NMR spectra. Magn. Reson. Chem. 40, 70–76 (2002).
25. de Lacaillerie JBD, Fretigny C, Massiot D, MAS NMR spectra of quadrupolar nuclei in disordered solids: The Czjzek model. J. Magn. Reson. 192, 244–251 (2008). [PubMed: 18362082]
26. Gaillac R, Pullumbi P, Courdet F-X, Melting of zeolitic imidazolate frameworks with different topologies: insight from first-principles molecular dynamics. J. Phys. Chem. C 112, 6730–6736 (2018).
27. Clupper DC, Hench LL, Crystallization kinetics of tape cast bioactive glass 45S5. J. Non. Cryst. Solids. 318, 43–48 (2003) .
28. Moghadam PZ, Li A, Wiggin SB, Tao A, Maloney AGP, Wood PA, Ward SC, Jimenez DF, Development of a cambridge structural database subset: A collection of metal–organic frameworks for past, present, and future. Chem. Mater. 29, 2618–2625 (2017).

29. Banerjee R, Phan A, Wang B, Knobler C, Furukawa H, O'Keeffe M, Yaghi OM, High-throughput synthesis of zeolitic imidazolate frameworks and application to CO_2 capture. Science 319, 939–943 (2008). [PubMed: 18276887]

30. Gan Z, Hung I, Wang XL, Paulino J, Wu G, Litvak IM, Gor'kov PL, Brey WW, Lendi P, Schiano JL, Bird MD, Dixon IR, Toth J, Boebinger GS, Cross TA, NMR spectroscopy up to 35.2T using a series-connected hybrid magnet. J. Magn. Reson. 284, 125–136 (2017). [PubMed: 28890288]

31. Siegel R, Nakashima TT, Wasylishen RE, Sensitivity enhancement of NMR spectra of halfinteger spin quadrupolar nuclei in solids using hyperbolic secant pulses, J. Magn. Reson. 184, 85–100 (2007). [PubMed: 17046297]

32. Kupce E, Freeman R, Adiabatic Pulses for Wideband Inversion and Broadband Decoupling, J. Magn. Reson. 115, 273–276 (1995).

33. Harris RK, Becker ED, Cabral de Menezes SM, Goodfellow R, Granger P, NMR nomenclature. Nuclear spin properties and conventions for chemical shifts (IUPAC Recommendations 2001), Pure Appl. Chem. 73, 1795–1818 (2001).

34. Spearing DR, ptchg: A FORTRAN program for point-charge calculations of electric field gradients (EFGs), Comput. Geosci 20, 615–624 (1994).

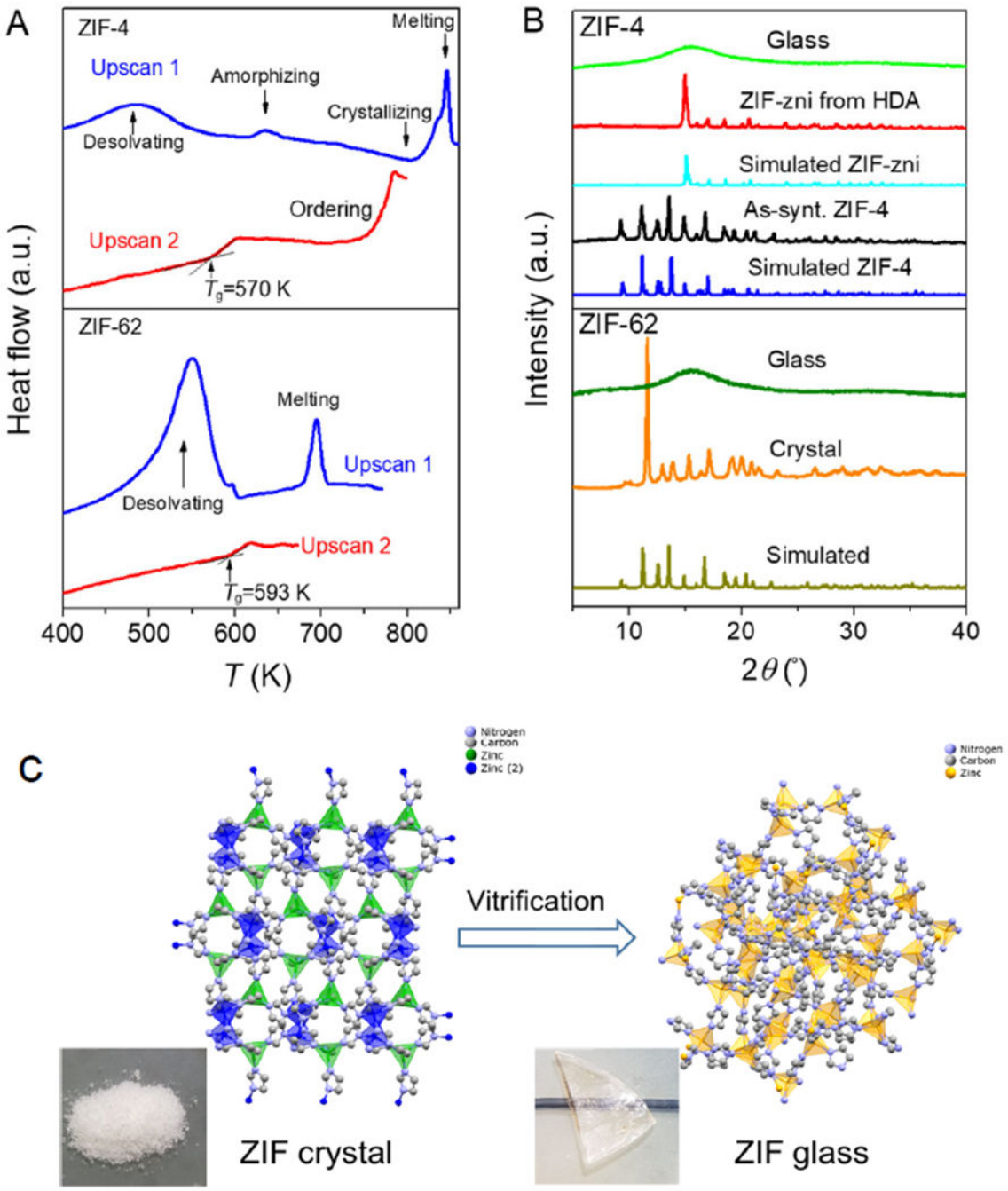

Fig. 1. Phase transitions, glass formation and glass transition for ZIFs.

(A) First and second DSC upscans for both ZIF-4 and ZIF-62, respectively. (B) XRD patterns of as-prepared ZIF-4 crystals, ZIF-zni crystals, ZIF-4 glass, ZIF-62 crystals and ZIF-62 glass. (C) Conceptual schematic representation of the structural change from crystalline ZIF (see powder sample) to its glassy state (see transparent bulk sample) during melt-quenching.

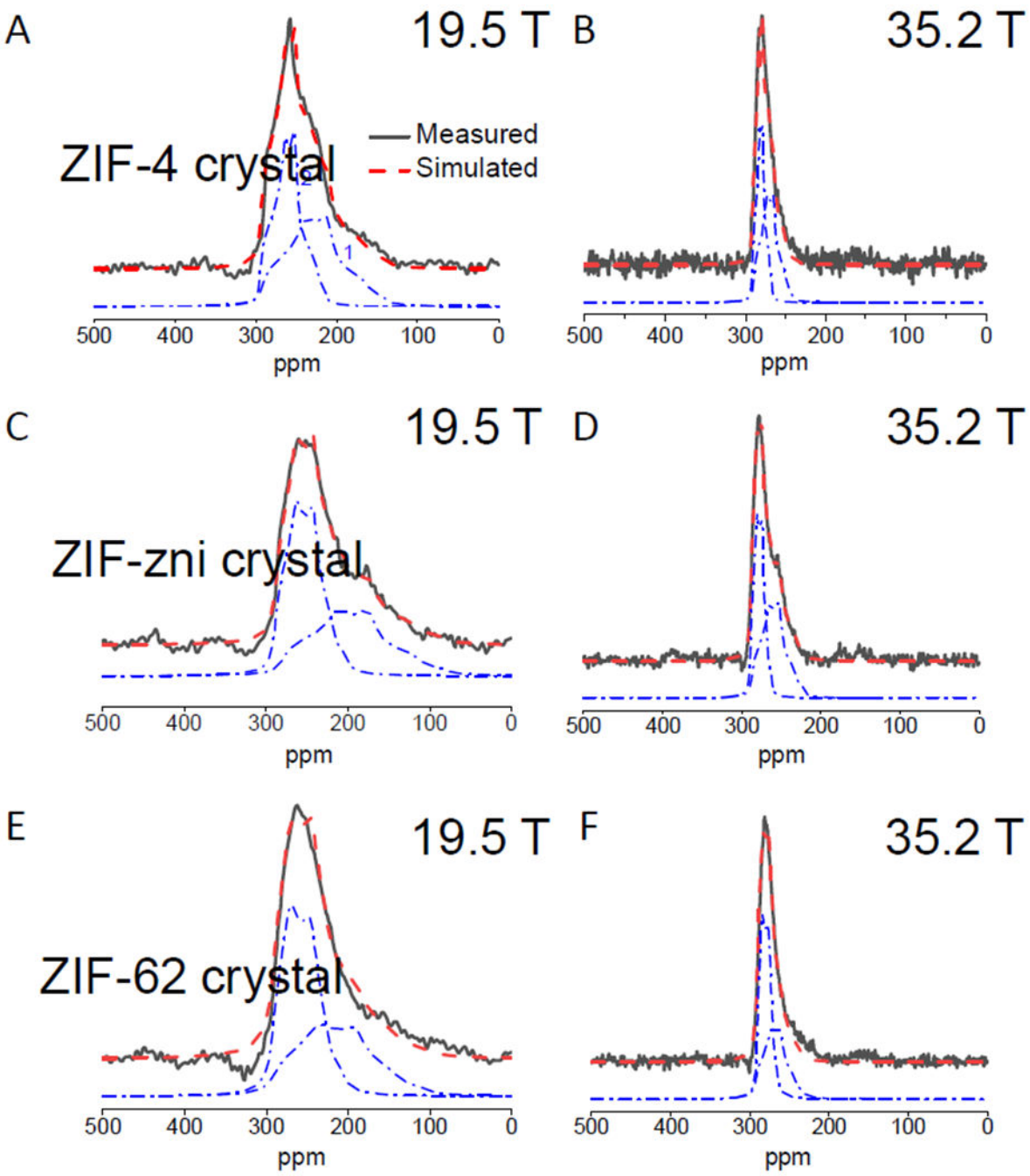

Fig. 2. Short-range order of crystalline ZIFs.

Experimental (solid black line) and simulated (dashed red line) ^{67}Zn MAS NMR spectra of crystalline ZIF-4 (A, B), ZIF-62 (C, D), and ZIF-zni (E, F) collected at 19.5 and 35.2 T. Individual simulation components (dot-dashed blue lines) are vertically offset for clarity.

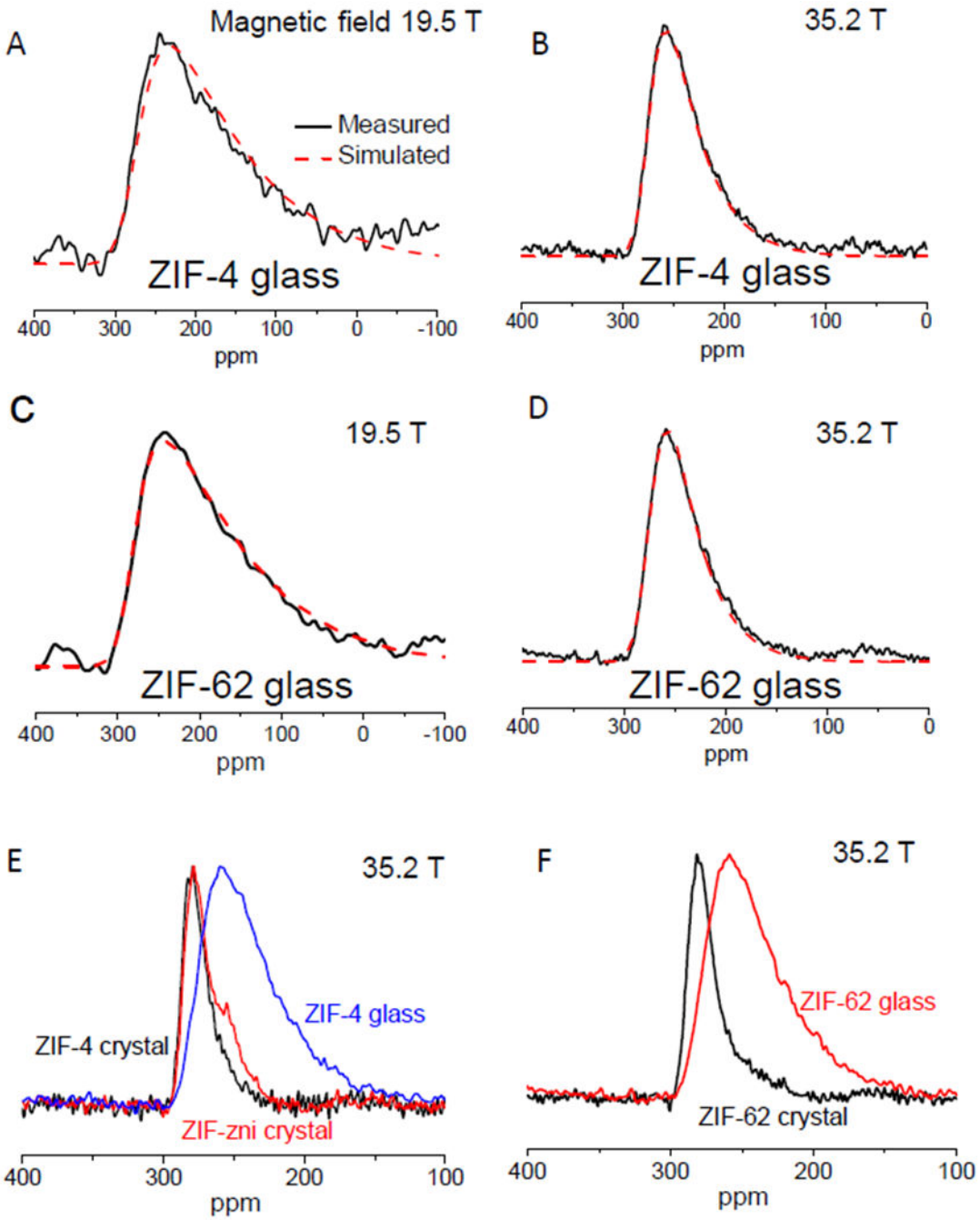

Fig. 3. Comparison of short-range structure between ZIF glasses and crystals.

Experimental (solid black line) and simulated (dashed red line) ^{67}Zn MAS NMR spectra for ZIF-4 glass (A, B) and the standard ZIF-62 glass (C, D) at different magnetic fields. Direct comparison of ^{67}Zn MAS NMR spectra collected at 35.2 T between ZIF-4 crystal, ZIF-zni crystal, ZIF-4 glass (E), as well as spectra of ZIF-62 crystal and glass (F).

Table 1.

^{67}Zn NMR parameters.

^{67}Zn MAS NMR line shape simulation parameters for crystalline and glassy MOFs.

MOF	Lattice site*	δ_{iso} (ppm)	C_Q ((±0.2MHz)	η_Q (±0.05)	Relative fraction (±5%)
ZIF-4 crystal	Zn1	296	5.1	0.6	46
	Zn2	295	3.7	0.6	54
ZIF-62 crystal	Zn1	297	5.8	0.5	48
	Zn2	296	4.0	0.4	52
ZIF-zni crystal	Zn1	288	6.0	0.6	46
	Zn2	290	4.0	0.5	54
ZIF-4 glass	Zn	277	6.9#	N/A	100
ZIF-62 glass	Zn	278	6.5#	N/A	100
ZIF-62b glass	Zn	277	6.8#	N/A	100

*Lattice sites correspond to those designated in structural refinements of ZIF-4, ZIF-62 and ZIF-zni, as reported in references [8,28,29].

#These values represent the root mean square quadrupolar product $\sqrt{\langle C^2_{Q\eta} \rangle}$.